INSTITUTE FOR NUCLEAR STUDY
UNIVERSITY OF TOKYO
Tanashi, Tokyo 188
Japan

INS-Rep.-403
Feb. 1981

Nuclear Physics Experiment at INS

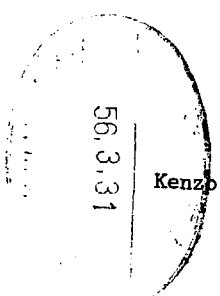

Kenzo Sugimoto

INS-Rep.-403
Feb. 1981

Nuclear Physics Experiment at INS

Kenzo Sugimoto

Institute for Nuclear Study, University of Tokyo
Midori-cho, Tanashi-shi, Tokyo 188

Present activities at the Institute for Nuclear Study (INS) are presented. Selected topics are from recent experiments by use of the INS cyclotron, experiments at the Bevalac facility under the INS-LBL collaboration program, and preparatory works for the Numatron project, a new project for the high-energy heavy-ion physics.

[Contents]

Presented at the Japan-Italy Symposium on Fundamental Physics, Tokyo, Jan. 27-30, 1981.

§1 Introduction

Present activities at the Institute for Nuclear Study (INS) are presented. Firstly, a brief sketch of activities in our country in the field of nuclear physics is given, since our institute is operated under the inter-university base: Locations of major universities and research institutes are shown in Fig. 1 in which the nuclear-physics research is active, together with locations of various accelerators. Altogether about 500 physicists are active in the experimental nuclear physics.

The Institute for Nuclear Study (INS) was established in 1955, in order to promote research activities in the nuclear and particle physics in our country. The facilities at the Institute are open to all researchers. At present, the staff members are 55 in the scientific works, 62 in the technical works, and 42 in the office and other works.

Four research divisions are active at the Institute:[1] the Low-Energy Physics Division, the High-Energy Physics Division, the Theoretical-Physics Division, and a Study Group for High-Energy Heavy-Ion Project, *i.e.*, the Numatron Project.

The accelerators in operation are an FM cyclotron (E_p = 52 MeV), an SF cyclotron (K = 68), and an electron synchrotron (E_e = 1.3 GeV). Historically, the FM cyclotron was the first one built at the Institute, which could also be operated as an ordinally cyclotron with a unique capability of variable energy. The electron synchrotron came into operation in 1961, and the energy has been boosted up to 1.3 GeV since 1966. The new SF cyclotron came into operation in 1974.

The layout of the electron-synchrotron facility is shown in Fig. 2. Three beam courses are provided in the experimental area, *i.e.*, γ1, γ2, and γ3. Recently, at the γ2 course, precision measurements on the nucleon-resonance character have been performed utilizing a polarized target or a proton polarization analyzer. Search for exotic states, *i.e.*, dibarion resonances, has also been performed by γ+d → p↑+n, and by γ+d↑ → p+n. At the γ3 course, photodisintegration studies on nucleus

targets have been performed utilizing the tagged-photon system and clear proton spectra from a quasifree nucleon-nucleon system have been found. Since the activity at the electron synchrotron is presented by Homma at this symposium, no further detail is given here.

The activities by use of the cyclotron facility are given in §2.

The Institute has also acted as a center to promote research programs of our country in the field of nuclear and particle physics: Preparatory studies were done at the Institute for the construction of the 12-GeV proton synchrotron and the related research programs at the Laboratory for High-Energy Physics (KEK); Activities conducted by the cosmic-ray research group at the Institute have led to the present-day expansion of the Institute for Cosmic Ray Research; Presently, preparatory works are actively going on for the construction of a high-energy heavy-ion accelerator complex, the "Numatron", and the related research programs. In this connection, an active participation to the Bevalac experiment at the Lawrence Berkeley Laboratory is promoted under the INS-LBL collaboration program.

Experimental results so far obtained by our group at the Bevalac facility are given in §3, and the Numatron project and its preparatory works are described in §4.

In order to support the research activities at the Institute, a computer network system for real-time data acquisition and processing has been installed. The system consists of two main computers, type FACOM M-180 IAD, the operation speed of which is 2.5 MIPS, with six terminal minicomputers.

The Institute has also helped to develop the applied science using nuclear technology: The beam of particles accelerated by the cyclotron has been used for bio-medical studies. The use of synchrotron radiation to the solid-state studies was initiated at the electron synchrotron in early 60's, and the activities have continued at the SOR facility, *i.e.*, an 300-MeV electron storage ring, located at the synchrotron laboratory (see Fig. 2).

§2 Recent Experiments by use of the INS cyclotrons

Presently, the nuclear-physics experiment is mainly performed by use of the sector-forcussed (SF) cyclotron. The K number of the cyclotron is 68, and the accelerated beams of particles so far obtained are shown in Table I. An atomic-beam-type polarized-ion source is equipped in the vertical injection line and polarized protons and deuterons can be accelerated.

The layout of the SF-cyclotron facility is shown in Fig. 3. Eleven beam courses are provided. Main measuring apparatus are a bombarding system for radio-isotope production, an on-line isotope separator, an in-beam gamma-ray goniometer, an 80-CM scattering chamber, a particle-correlation chamber, and a QDD-type high-resolution spectrograph. The QDD-type spectrograph is a broad-range type with $E_{max}/E_{min} = 1.35$ and characterized by a high resolution of $(p/\Delta p)_{max} = 10^4$ with a relatively small dispersion and a small horizontal magnification. A 75-CM radius air-core beta-ray spectrograph has also been installed in a separate iron-free laboratory.

In the following, four topics are discussed among the results recently obtained.

2-1 Deep-hole states

Systematic studies have been performed on the deep-hole states *via* (p, d), (d, t), and (^{3}He, α) reactions on Sn and Sm isotopes. Historically, by looking at a deuteron spectrum from the ^{115}Sn(p, d)^{116}Sn reaction, Sakai and Kubo[2] noticed a possibility to study deep-hole states *via* pick up reactions (see Fig. 4-a)). This possibility was realized especially by using the (^{3}He, α) reaction[3), 4] as shown in Fig. 4-c) and in Fig. 4-d). This is a clear experimental evidence for that the shell-structure orbits persist in deeply-bound states even in heavy nuclei.

In Fig. 5, the results obtained on the Sn isotopes are summarized.[4] It is interesting to see that the neutron separation energy from the

deeply-bound states is independent of mass number A, while that from the valance orbits is dependent of A. The results have stimulated interests and induced extensive works at various laboratories.

2-2 Systematics on level structures of nuclei in the transitional regions

It has been a long-standing problem whether there would be a systematic trend of level structures due to collective modes throughout the region from spherical to deformed and how to understand it theoretically if it were. Sakai[5] pointed out such a possible trend so called as a quasi-band structure, from the available data in 1967.

So far data accumulated[6] at our institute on nuclei around A∿80, such as Se, Kr and Sr, and also around A∿120, such as Sn and Cd, by the methods of the in-beam gamma-ray spectroscopy and of the particle spectroscopy on the (p, d) and (p, t) reactions. As an example, the level structures on nuclei around A∿80 are shown in Fig. 6-a)~c). If one compares the level structures with those expected from schematic models of vibrational limit and of rotational limit shown in Fig. 7, one can notice the observed ones lie between those limits. The same situation is also found in the region around A∿120.

2-3 ^{6}Li induced reaction

The SF cyclotron has been equipped with an internal cold-cathod Penning ion source which can deliver a high-intensity beam of Li^{3+} ions.[7] A piece of single-crystal LiF has been used as the charging material in the arc chamber of the ion source. The energy of the Li-ion beam provided by our SF cyclotron is E ∿ 80 MeV and higher than that provided by the conventional tandem Van de Graaff machines.

In taking advantage of such a high-energy beam, a study on the $^{16}O(^{6}Li, d)^{20}Ne$ reaction has been done.[8] A deuteron energy spectrum is shown in Fig. 8-a). The line spectrum resulted from α-transfer to the states in the ground-state band of ^{20}Ne is clearly seen, which is free from continuum of deuterons due to ^{6}Li break-up, in contrast to the

spectra obtained by the lower incident energies. The angular distributions are shown in Fig. 8-b), which can be well fitted by DWBA predictions with an assumption of direct α-cluster transfer, in contrast to the other works so far reported. The analyses yielded the spectroscopic factors in agreement with shell-model predictions.

2-4 Spin-flip asymmetry in the $^{12}C(\vec{p}, p')^{12}C^{*}$ reaction

In the inelastic scattering of protons by ^{12}C leading to the 1st-excited state (2^{+}, 4.43 MeV), the spin-flip probability of protons can be determined by measuring the gamma-ray intensity in the direction normal to the reaction plane. This is a well known experimental procedure following the Bohr's theory. When polarized protons are utilized, one can determine not only the spin-flip probability (SF) but also the spin-flip asymmetry (SFA) besides the differential corss section (σ_o) and the asymmetry (A), *i.e.*, the left-right asymmetry of inelastically scattered protons by incidence of polarized protons. Then one can experimentally decompose the process into the partial cross sections using the following relations:

$$\sigma_o = (\sigma_{++} + \sigma_{+-} + \sigma_{-+} + \sigma_{--})/2$$
$$A = (\sigma_{++} + \sigma_{+-} - \sigma_{-+} - \sigma_{--})/2\sigma_o$$
$$P = (\sigma_{++} - \sigma_{+-} + \sigma_{-+} - \sigma_{--})/2\sigma_o$$
$$SF = (\sigma_{+-} + \sigma_{-+})/2\sigma_o$$
$$SFA = (\sigma_{+-} - \sigma_{-+})/(\sigma_{+-} + \sigma_{-+}) = (A - P)/2(SF)$$

where σ_{+-} (σ_{-+}) is the partial differential cross section for the process from the initial spin up + (down -) to the final spin down - (up +), and σ_{++} (σ_{--}) is for the non spin-flip process. Here the *s* axis is chosen in normal to the reaction plane. Results of such measurements[9] are shown in Fig. 9. This is an example of the effective use of the polarized beam to the study of reaction mechanisms.

§3 Experiments at the Bevalac Heavy-ion Facility

Since 1974, a group of Japanese physicists has participated experiments at the Bevalac high-energy heavy-ion facility at the Lawrence Berkeley Labolatory (LBL). As an extension of the activities, the INS-LBL collaboration program started in 1979 as a five-year program. The Bevalac facility has so far successfully accelerated heavy-ion beams of C, O, N, Ne and Ar up to 2 GeV/nucleon, and hes given a unique opportunity to study a new domain of physics with use of relativistic heavy ions.

A nucleus-nucleus collision at high energies can be characterized by a participant-spectator picture: The collision process is schematically drawn in Fig.10-a) in the center-of-mass system, and the distribution of emitted particles in the rapidity "y" is qualitatively given in Fig.10-b), where y_P and y_T are the projectile and target rapidities. In such collisions, objectives to study are, therefore, the projectile or target fragments on the one side and the overlap region involving participant nucleons on the other side. Interesting high energy- and matter-density states of nuclear matter can be expected to be realized at the overlap region, even though no convincing experimental evidence has been found so far for anything remotely unusual.

In the following, two topics are discussed from the experiments so far performed under our collaboration program.

3-1 Particle spectra at large angles in high-energy nuclear collisions

Productions of π^+, π^-, p, d, ^{3}H, ^{3}He, and ^{4}He have been studied at large angles in high-energy nuclear collisions.[10)~15)] The experimental setup is shown in Fig.11. Particles of momenta from a few 100 MeV/nucleon to a few GeV/nucleon were measured by a magnetic spectrometer at angles from 10° to 145°. Besides the magnetic spectrometer, three sets of tag counter telescopes were provided to detect the associated multiplicity of each event and also to study the particle correlations in plane and out of plane with the spectrometer.

In the laboratory frame, the projectile fragments are mostly emitted in a very small forward cone with high energies while the target fragments are stayed in low energies, and particles from the overlap region tend to be emitted over a wide range of angle in relatively high energies. In the present experiment, light particles emitted at large angles in high energies have been measured, so that the data mostly reflected features of the overlap region.

Heavy-ion beams used were C, Ne, and Ar at 800 MeV/nucleon, to study the projectile mass dependences. Targets were elements of nearly equal mass to the projectiles for equal-mass nuclear collisions, *i.e.*, C + C, Ne + NaF, and Ar + Kcl, and heavy-mass elements such as Cu and Pb. Dependences on the incident energy have been studied in the case of Ne projectiles with 400 MeV/nucleon and 2.1 GeV/nucleon. For comparisons, proton incident collisions have also been studied with 0.8- and 2.1-GeV protons on various targets.

3-1-1 Inclusive spectra

Firstly, results of the inclusive-type measurements are discussed. Proton momentum spectra in the Ar + Kcl collisions are shown in Fig. 12. At forward angles, the spectra show a "shoulder-arm" shape. The turning point is located at a momentum close to a peak observed in the proton-incident collisions as due to the pp or pn quasi-elastic scattering. In the arm region, no proton would be kinematically allowed if a nucleus-nucleus collision were merely a simple assembly of nucleon-nucleon collisions. Thus, the spectra in such kinematical domains especially contain the nuclear effects, *e.g.*, effects of internal motion, short-range correlation, cumulative effect, multiple scattering, *etc.*

The energy distributions of protons and pions[11), 12)] emitted at c.m. 90° for 800-MeV/nucleon incidence are shown in Fig. 13. The proton spectra are characterized by a "shoulder-arm" type with an exponential fall-off at high energies as discussed, while the pion spectra are almost simple exponential. The inverse of the exponential slope, E_o, for protons is systematically larger than that for pions, *i.e.*, E_o = 70~90 MeV for

protons and 60~70 MeV for pions, and E_o increases monotonically with the beam energy as shown in Fig. 14. A saturation feature of E_o towards higher beam energies is observed as $E_o \lesssim m_\pi c^2 = 140$ MeV. The E_o is also systematically larger for larger-mass combinations between projectile and target, *e.g.*, in proton spectra, $E_o = 68$ MeV for C + C and $E_o = 87$ MeV for Ar + Pb (see Fig. 13).

The proton angular distributions show sharp forward and backward peaking in the c.m. frame and the anisotropy for protons increases with the beam energy, while those for pions are less anisotropic and does not show a strong beam-energy dependence.

The spectrum shapes of the composite fragments, d, ^{3}H, *etc.*,[13] are well explained by the A^{th} power of the observed proton spectra, where A is the mass number of the composite fragments, as shown in Fig. 15. This fact strongly indicates the importance of the final-state interactions: According to a simple phase-space consideration, the probability of forming deuterons at velocity $\vec{V}_d$ is proportional to the product of probabilities of finding protons and deutrons at the same velocity; $P_d(\vec{V}_d) \propto P_p(\vec{V}_p=\vec{V}_d)\cdot P_n(\vec{V}_n=\vec{V}_d)$. This is the well-known concept of coalscence. In high energy nuclear collisions, the spectrum of neutrons can be approximated by that of protons. Thus, one can expect for the composite fragment of mass A,

$$E_A(d^3\sigma_A/d^3P_A) = C_A[E_p(d^3\sigma_p/d^3P_p)]^A,$$

where $P_A = A\cdot P_p$, and C_A is a constant, the coalescence coefficient. The relation held very well at all fragments and all angles, and it turned out that the coefficient C_A is almost independent on the beam energy but dependent on the fragment type and the projectile and target masses. This fact told us about the geometrical aspect and dynamics of the final-state interactions but not about the formation or dynamics of the primary stage. Sizes of the interaction region were evaluated from the determined coalescence coefficients.

3-1-2 Two-proton correlations

Energy and angular correlations of two protons emitted in high-energy

nuclear collisions have been studied.[14] Three sets of tag counter telescopes were provided at angles $\theta = 40°$ and $\phi = 180°$(R), 90°(U), and 270°(D), the beam axis being the z axis, and the magnetic spectrometer was located at $\phi = 0°$ and rotated between $\theta = 15°$ and 110°. The $\theta = 40°$ corresponds to $\theta_{c.m.} \sim 90°$ in the nucleon-nucleon c.m. frame. Protons of energies, $E_p \gtrsim 200$ MeV were counted by the telescopes. From the coincidence counts between the spectrometer S and the respective counter telescopes, R, U and D, a ratio $C(\theta, p)$ was determined;

$$C(\theta, p) \equiv 2\,\frac{\overline{S(\theta, p)\cdot R}/R}{\overline{S(\theta, p)\cdot U}/U + \overline{S(\theta, p)\cdot D}/D},$$

where θ and p are the angle and momentum of a proton detected by the spectrometer. The quantity $\overline{S(\theta, p)\cdot R}$ indicates the coincidence counts between the spectrometer and the R telescope, and the $\bar{R}$ indicates the single counts of the R telescope, and so on. The ratio C can be called the degree of coplanarity, because the coplanar two-proton emission is favored when $C > 1$.

Contour maps of the observed $C(\theta, p)$, displayed in the plan of p_η^* and $p_\perp^*$ of emitted protons in the nucleon-nucleon c.m. frame, are shown in Fig. 16, for collisions of C + C and Ar + KCl at 800-MeV/A incidence. The dotted circle indicates the free nucleon-nucleon elastic-scattering kinematics. The value of C has a peak right on the circle at the opposite side of the R telescope. The data thus clearly show the existence of pp quasi-elastic scattering in the nucleus-nucleus collisions. Analyses of the data indicated that the fractions, P, of the clear knock-out process for protons emitted at $\theta_{c.m.} \sim 90°$ were $P \sim 50\%$ for all the studied equal-mass nuclear collisions.

3-1-3 High-multiplicity events

High-multiplicity events (HME) would be suitable to study nucleus-nucleus collisions at small impact parameters. To select high-multiplicity events, nine sets of tag counter telescopes were placed at $\theta = 40°$. Each telescope detected particles of high energies, typically $E_p > 100$ MeV. Angular distributions of high-energy protons ($E_p > 100$ MeV) in collisions

of 800-MeV/nucleon Ar + Pb are shown in Fig. 17 for inclusive events and HME.[15] The inclusive spectrum shows a strong forward peaking, but as increasing the multiplicity the forward emission is highly suppressed. The quantity M in the figure indicates the tag counter multiplicity used to bias toward higher multiplicities, *e.g.*, M = 5 corresponded to a total multiplicity of approximately 49. In Ar + Pb collisions, complete suppression of projectile fragments for HME can be clearly seen if one plot the data as shown in Fig. 18, in which the proton invariant cross sections are plotted in the plane of rapidity y and the normalized transverse momentum ($p_T/m_p c$). Here both inclusive events and HME, $M \geq 5$, are shown for comparison. Each contour line connects the same invarient cross section, and two consecutive thick curves differ by a factor of 10 in cross section. For inclusive events, a strong influence from both projectile and target fragments can be seen in the small p_T region, while such an influence completely disappears for HME. Complete suppression of projectile fragments in HME is consistent with the picture that HME are selecting small impact parameters. It is interesting to note that the angular distribution of high-energy protons in HME is almost isotropic in a moving frame whose rapidity $y_o \simeq 0.43$. The evidence that Pb is very opaque may play an important role in future experiments involving U + U.

3-2 Threshold pion production in nuclear collisions

Pion productions at 0° in Ne + NaF collisions have been studied at incident energies from 125 to 400 MeV/nucleon.[16] A 180° magnetic spectrometer was used, as shown in Fig. 19, which has permitted measurements of both π^+ and π^- with kinetic energy between 34 and 155 MeV in the laboratory flame.

A sharp peak in the π^- production and the π^-/π^+ ratio has been found for pions of velocity close to the projectile velocity. Typical pion spectra are shown in Fig. 20 for 258-MeV/nucleon Ne + NaF collisions at $\theta = 0° \pm 3°$. The peak in the π^-/π^+ ratio can be qualitatively explained in terms of Coulomb distortion of pion wave functions in the vicinity of the projectile charge. Further detailed studies on the Coulomb effects may be effective to elucidate the microscopic structure of heavy-ion interaction region.

The observed differential cross section at 0° varied by about four orders of magnitude over the beam-energy range studied. The rapid rate of change of the cross section is not in accord with the first-collision Fermi-gas production model.

Concerning to the study of low-energy pion productions, it is noted that a bump in the positive-pion yield has been observed[17] at c.m. 90° at $p_T \sim 0.5\ m_\pi c$ for 0.8-GeV/nucleon Ne + NaF collisions. This 90° bump in π^+ production is denoted to be specific for the nucleus-nucleus collisions in comparison with the pion production in the pp collisions, though no definite interpretation is yet available.

§4 The Numatron Project

A group of physicists in Japan has proposed a new project to construct a high-energy heavy-ion accelerator complex, named "Numatron".[18), 19] The aim of the project is to open a new field of physics with use of heavy ions of all elements accelerated up to a few GeV/nucleon.

From the nuclear-physics point of view, interesting new phenomena can be expected to be realized in getting into a domain which lies beyond the sound velocity of nuclear matter and beyond the meson-production thresholds, as discussed in §3. It can also be expected that a vast number of new isotopes far from the stability line will be effectively produced, *e.g.*, by the projectile-fragmentation process.

A study group for the Numatron project was assembled in 1976 at INS, and the preparatory works have been done including the detailed design study of the accelerator complex and related technical developments.

4-1 Proposed facility

A plan view of the proposed accelerator complex, the Numatron,[19), 20)] is shown in Fig. 21. The accelerator complex consists of a heavy-ion linear-accelerator system, as the injector of 10-MeV/nucleon ion beams to the following synchrotron, and a two-ring synchrotron system. The two-ring synchrotron system is introduced in order to obtain reliably the final intensities of heavy-ion beams of $\sim 10^{10}$ ions/s, by use of the beam-accumulation technique in the 1st ring. The operation scheme of the system is as shown in Fig. 22. In the 1st ring, ion beams injected from the linac are accumulated by a combination of the multiturn-injection and RF-stacking methods, then accelerated up to 150 MeV/nucleon and extracted by the one-turn ejection method. After passing through the final-stage stripper, fully stripped ions are injected into the 2nd ring and further accelerated. The expected intensities of various ions are tabulated in Table II. The ion-mass *vs.* energy capability of the present design is shown in Fig. 23, together with those of the other existing or proposed projects.

4-2 Preparatory works

In a construction of high-energy heavy-ion accelerator, one encounters a number of new accelerator-physics and engineering problems different from the proton-accelerator case; problems on the ion source, the low-velocity linac, the high-vacuum system needed to avoid the charge-exchange processes of heavy ions, and methods to obtain a high intensity of the heavy-ion beam in spite of the low-intensity-beam capability of the present-day ion-source technique. Our group has devoted efforts to study such problems in detail.

A test accumulation ring for heavy ions, named "Tarn", has been constructed[21)] in order to develope especially the heavy-ion-beam accumulation technique, as shown in Fig. 24. The heavy-ion beams, *e.g.*, 8.5-MeV/nucleon N^{5+}, accelerated by the INS-SF cyclotron were injected and accumulated in the Tarn. The vacuum in the ring is required to be 10^{-10} Torr for survival of 90% ions during the stacking time of 1 sec for

the charge-exchange cross section of N^{5+}, $\sim 3 \times 10^{-17}$cm^2. The vacuum of the Tarn has been attained to $\sim 2 \times 10^{-11}$ Torr, and $< 10^{-10}$ Torr in routine, which has been confirmed from the lifetime of the circulating beam. Both the multi-turn injection and the RF stacking of ion beams have been tested successfully. Further studies are in progress especially on the transverse resistive-wall instability for low-velocity and high-density ion beams, which is a limiting factor for the intensity of the accumulated ion beam.

The proposed Numatron project is a 5-year plan in its construction. It is hoped that the project will be fully approved in the near future, even though the site for the project and associated problems have not been settled yet.

[References]

1) Annual Report 1979, Institute for Nuclear Study, University of Tokyo.
2) M. Sakai and K. Kubo, Nucl. Phys. A185 (1972) 217.
3) M. Sakai, M. Sekiguchi, F. Soga, Y. Hirao, K. Yagi and Y. Aoki, Phys. Letter 51B (1974) 51.
4) M. Sekiguchi, Y. Shida, F. Soga, Y. Hirao and M. Sakai, Nucl. Phys. A278 (1977) 231.
5) M. Sakai, Nucl. Phys. A104 (1967) 301.
6) N. Yoshikawa, Y. Shida, O. Hashimoto, M. Sakai and T. Numao, Nucl. Phys. A327 (1979) 477.
7) T. Tanabe, Y. Ohshiro and K. Sato, Nucl. Instr. and Meth. 178 (1980) 315.
8) T. Tanabe, M. Yasue, K. Sato, K. Ogino, Y. Kadota, Y. Taniguchi, K.Makino and M. Tochi, Phys. Letter (in press).
9) T. Fujisawa, N. Kishida, T. Kubo, T. Hasegawa, M. Sekiguchi, N. Ueda, M. Yasue, Y. Wakuta and A. Nagao, Contributed Papers, Fifth International Symposium on Polarization Phenomena in Nuclear Physics, Santa Fe (1980) 2.50.
10) S. Nagamiya, I. Tanihata, S. Schnetzer, W. Brückner, L. Anderson, O. Chamberlain, G. Shapiro, and H. Steiner, J. Phys. Soc. Japan, Suppl. 44 (1978) 378.
11) S. Nagamiya, L. Anderson, W. Bruckner, O. Chamberlain, M.-C. Lemaire, S. Schnetzer, H. Steiner, I. Tanihata, Phys. Letter 81B (1979) 147.
12) I. Tanihata, S. Nagamiya, O. Chamberlain, M.-C. Lemaire, S. Schnetzer, G. Shapiro, and H. Steiner, Phys. Letter 87B (1979) 349.
13) M.-C. Lemaire, S. Nagamiya, S. Schnetzer, H. Steiner, and I. Tanihata, Phys. Letter 85B (1979) 38.
14) I. Tanihata, M.-C. Lemaire, S. Nagamiya, and S. Schnetzer, Phys. Letter 97B (1980) 363.
15) S. Nagamiya, M.-C. Lemaire, S. Schnetzer, H. Steiner and I. Tanihata, Phys. Rev. Letter 45 (1980) 602.
16) W. Benenson, G. Bertsch, G.M. Crawley, E. Kashy, J. Nolen, Jr, H. Bowman, J.G. Ingersoll, J.O. Rasmussen, J. Sullivan, M. Koike, M. Sasao, J. Peter and T.E. Ward, Phys. Rev. Letter 43 (1979) 683; [Errata, Phys. Rev. Letter 44 (1980) 54].
17) K. Nakai, J. Chiba, M. Sasao, I. Tanihata, H. Bowman, S. Nagamiya and J.O. Rasmussen, Phys. Rev. C20 (1979) 2210.
18) K. Sugimoto, S. Nagamiya, M. Sano, J.-I. Fujita, Y. Hirao, Butsurigakkai-shi (publication of Phys. Soc, of Japan, in Japanese) 30 (1975) 333.
19) NUMATRON -- High-Energy Heavy-Ion Facility, ed. Y. Hirao, INS-NUMA-5 (1979); Numatron, the acronym of nuclear-matter-tron.
20) Y. Hirao, J. Phys. Soc, Japan, Suppl. 44 (78) 594; Y. Hirao, IEEE Trans. NS-26 (1979) 3736.
21) Y. Hirao, K. Chida, T. Hattori, T. Hori, T. Katayama, A. Mizobuchi, M. Mutou, T. Nakanishi, N. Noda, K. Omata, N. Tokuda, H. Tsujikawa, S. Watanabe, S. Yamada, M. Yoshizawa, E. Ezura, H. Sasaki, and A. Miyahara, IEEE Trans. NS-26 (1979) 3730;
Tarn, the acronym of test-accumulation-ring for the Numatron Project.

Energy and intensity of the extracted beams of the SF cyclotron so far achieved.

Ion	Energy (MeV)	Extracted Beam Current (eμA)	Comments
p	48	30	
p^+	48	0.06	
d	33	30	
d^+	33	0.08	
$^3He^{++}$	90	25	
$^4He^{++}$	68	30	
$^6Li^{++}$	45	0.1	LiF+Xe, natural
$^6Li^{3+}$	75	2	LiF+Xe, enriched
$^7Li^{3+}$	80	2.2	LiF+Xe
$^{11}B^{4+}$	98	0.003	BN+Xe
$^{12}C^{4+}$	88	3.5	CO_2
$^{14}N^{4+}$	40	5	N_2, 3rd harmonic
$^{14}N^{5+}$	115	4.3	N_2
$^{16}O^{5+}$	104	3.5	CO_2
$^{16}O^{6+}$	130	0.3	CO_2
$^{20}Ne^{4+}$	52	0.3	Ne
$^{20}Ne^{5+}$	60	0.1	Ne, 3rd harmonic
$^{20}Ne^{6+}$	115	1.5	Ne
$^{20}Ne^{7+}$	150	0.02	Ne
$^{40}Ar^{8+}$	104	0.001	Ar

The extracted beam current is not necessarily achieved at the energy quoted in the table.

Table I Beam of particles so far accelerated by the INS-SF cyclotron

CAPABILITY OF THE NUMATRON

Ion	Intensities					
	LINAC 300 KEV/NUCL.	LINAC 1.6 MEV/NUCL.	LINAC 10^{-2} MEV/U	1ST SYNCHROTRON 50~250 MEV/U	2ND SYNCHROTRON 1.3	2ND SYNCHROTRON 4.3 GEV/U
H	1×10^{16}	1×10^{16}	1×10^{16}	1×10^{11}		1×10^{11}
Ar	1×10^{15}	1×10^{15}	1×10^{15}	3×10^{10}		3×10^{10}
Kr	5×10^{14}	5×10^{14}	5×10^{14}	2×10^{10}		2×10^{10}
Xe	1×10^{14}	1×10^{14}	1×10^{14}	1×10^{10}		1×10^{10}
U	1×10^{12}	5×10^{11}	5×10^{11}	5×10^{9}*		3×10^{9}*

* INTENSITIES ARE LIMITED BY ION SOURCE, WHILE OTHERS IN THE SYNCHROTRONS ARE LIMITED BY SPACE CHARGE EFFECTS WHERE BUNCHING FACTOR IS ASSUMED AS 0.2. IN THE RANGE OF 50 ~ 250 MEV/U, THE 2ND SYNCHROTRON FUCTIONS AS A STRETCHER.

Table II Expected intensities of various ion beams by the Numatron.

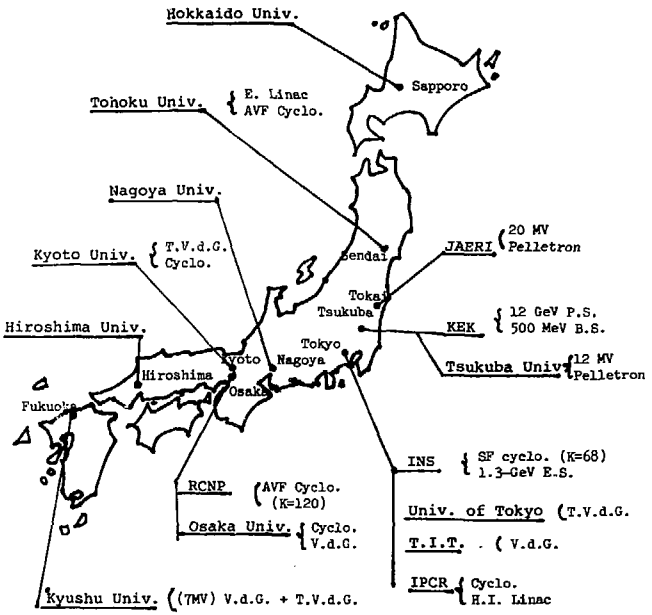

Fig.1 Major activities in Nuclear Physics in Japan.

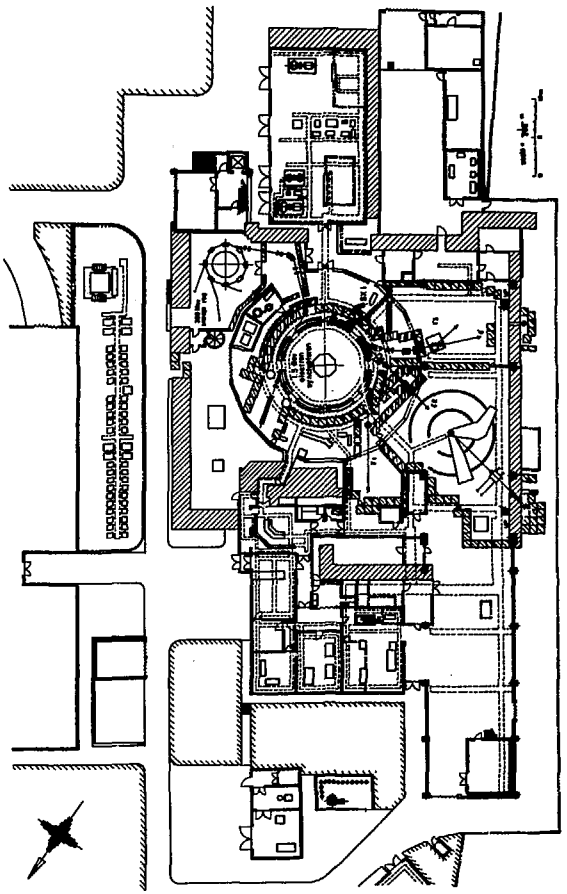

Fig.2 Plan view of the INS 1.3-GeV electron-synchrotron laboratory.

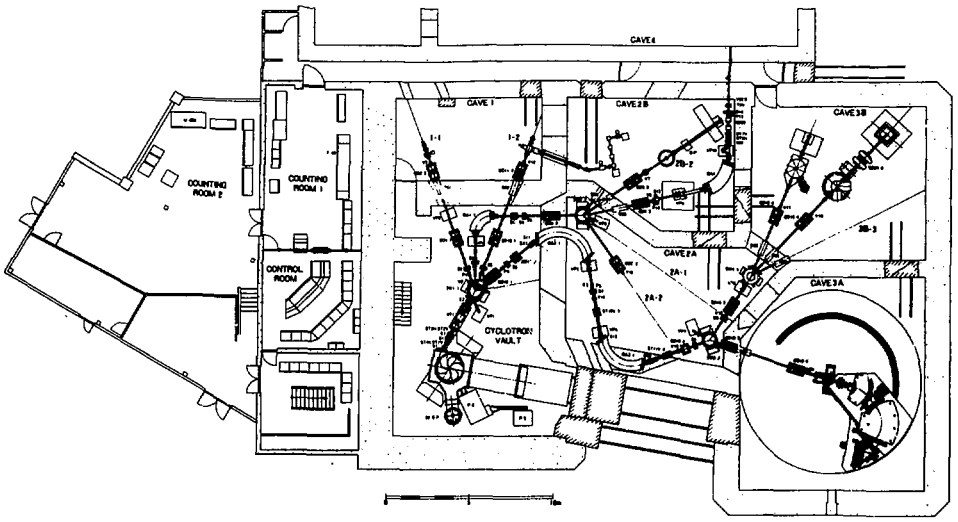

Fig.3 Plan view of the INS SF-cycloton laboratory.

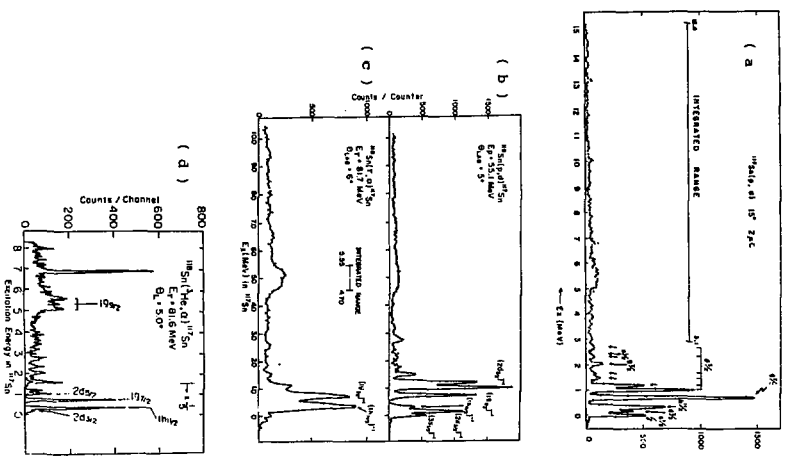

Fig.4 Deuteron and α-particle spectra of (p,d) and (^{3}He,α) reactions on Sn isotopes.

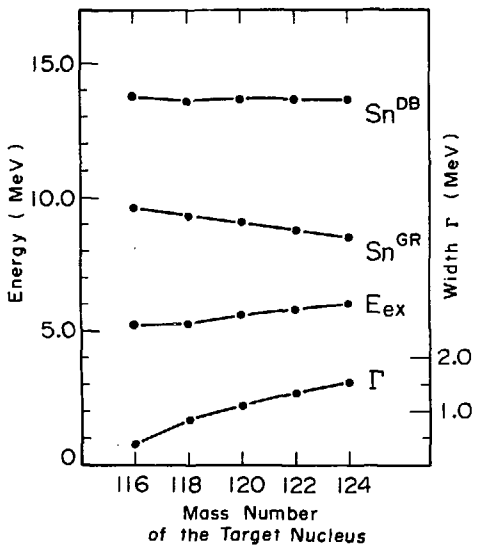

Fig.5 Mass-number dependence of the excitation energy(E_{ex}) and the width(Γ) of the deep-hole state on Sn isotopes, and the neutron seperation energy of the deeply-bound state (Sn^{DB}) and the ground state(Sn^{GR}).

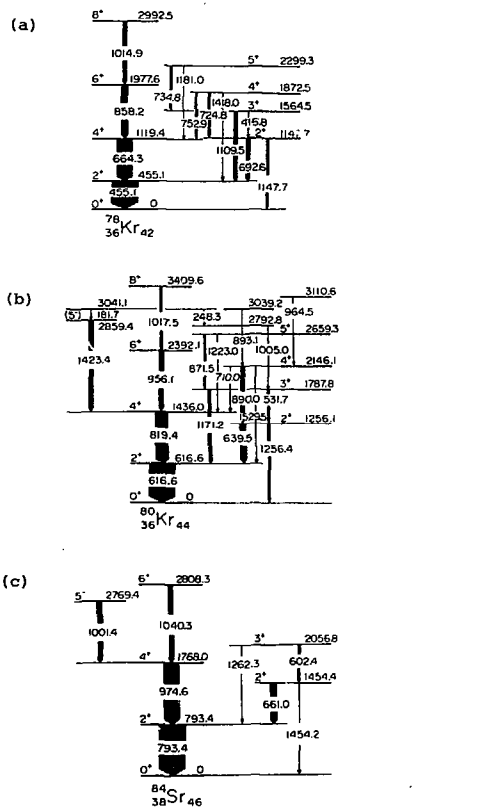

Fig.6 Level schemes for a) ^{78}Kr, b) ^{80}Kr and c) ^{84}Sr.

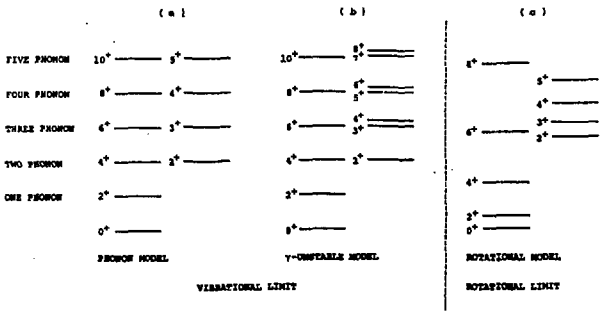

Fig.7 Schematic level schemes in the vibrational or the rotarional limits.

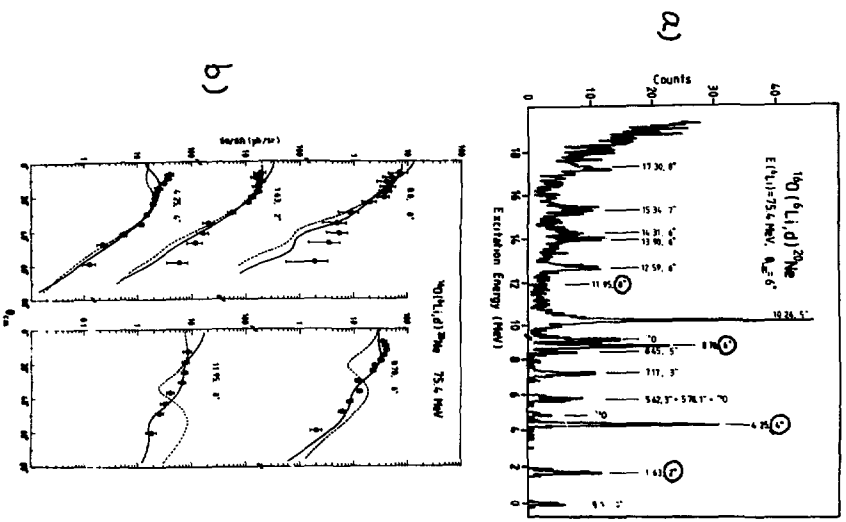

Fig.8 a) Deuteron energy spectrum, and b) angular distribution of the $^{16}O(^{6}Li,d)^{20}Ne$ reaction.

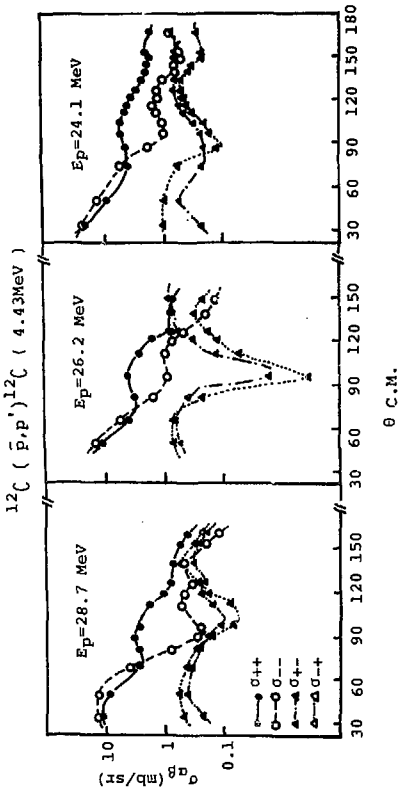

Fig.9 Decomposition into the partial cross sections, σ_{++}, σ_{--}, σ_{+-}, and σ_{-+}, of the $^{12}C(p,p')^{12}C^*$ reaction.

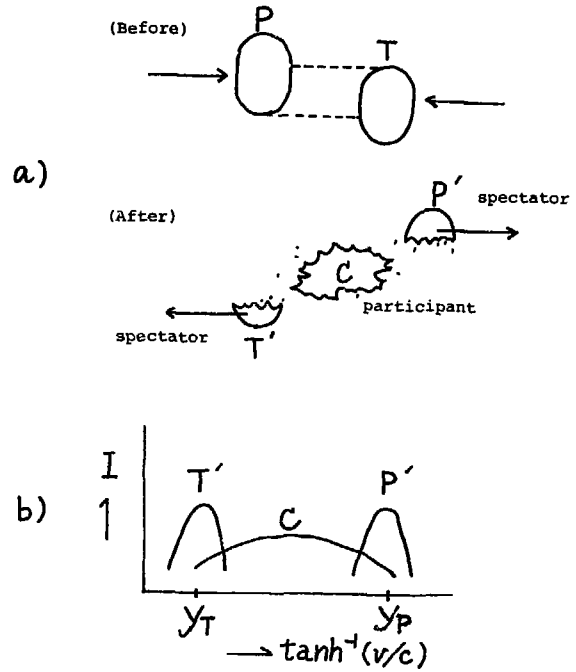

Fig.10 Participant-spectator picture for high-energy nucleus-nucleus collisions.

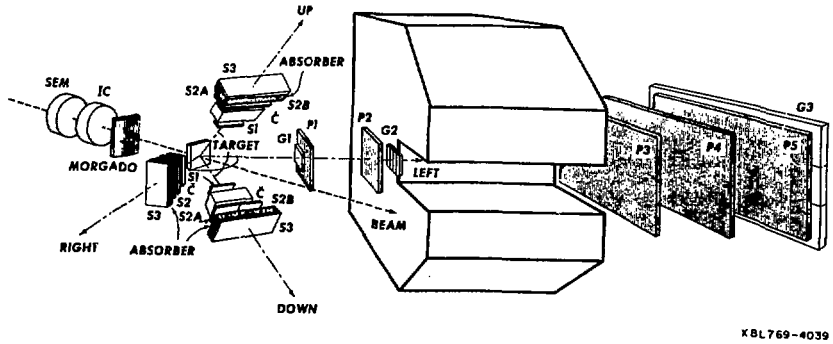

Fig.11 Experimental setup for particle production at large angles in high-energy nuclear collisions.

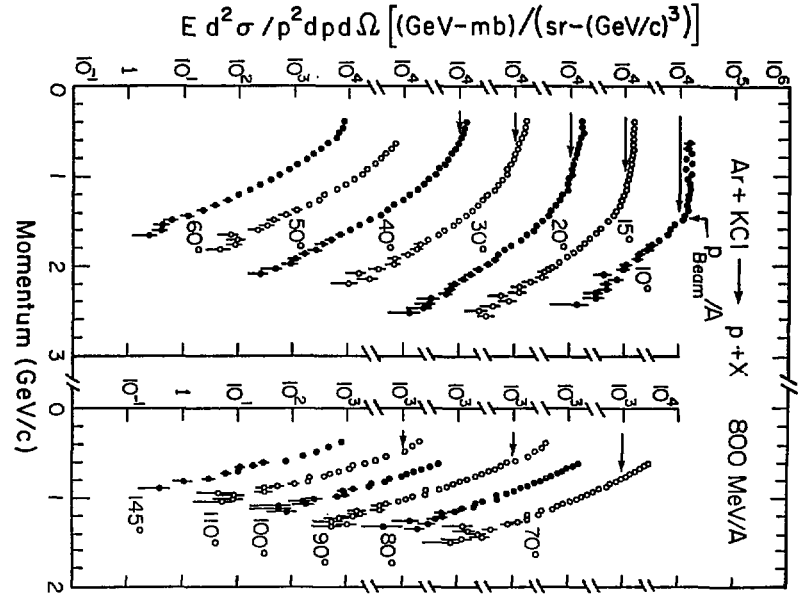

XBL8011-2393

Fig.12 Proton momenturm spectra in Ar + KCl collisions.

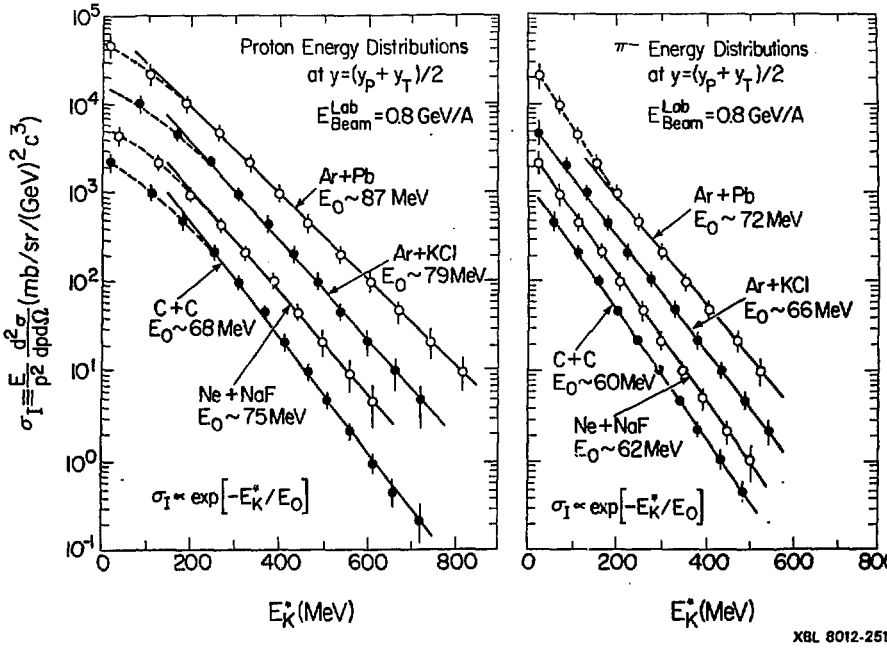

Fig.13 Energy spectra for protons and pions at c.m. 90°.

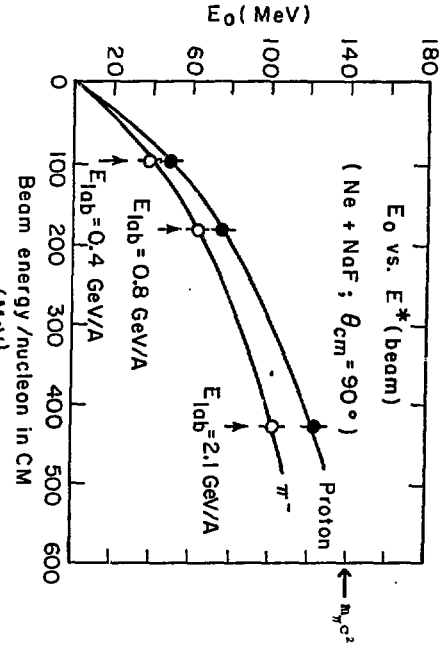

Fig.14 E_0 in $\sigma \propto \exp[-E_K^*/E_0]$ for protons and pions.

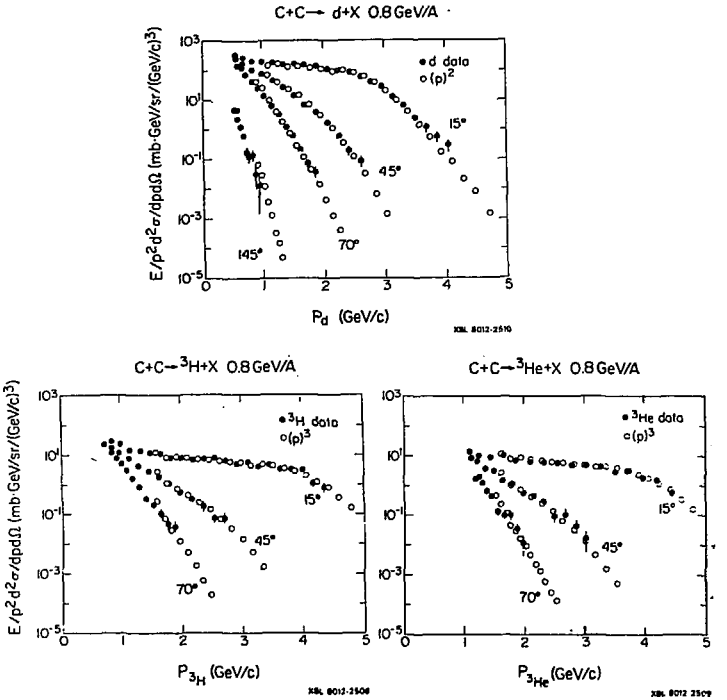

Fig.15 Spectra of d, ^{3}H and ^{3}He in 800-MeV/nucleon C + C collisions, compared with the A^{th} power of the observed proton spectra.

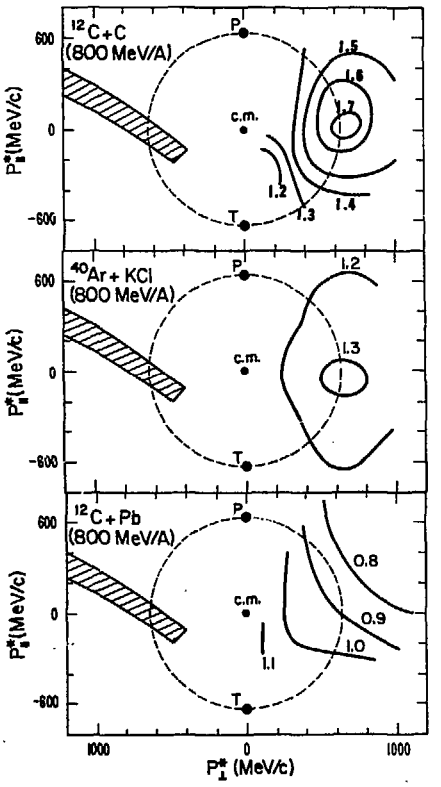

XBL 793-7568

Fig.16 Contour plot of the coplanarity $C(\theta,\rho)$ of two-proton emissions in the nucleon-nucleon c.m. frame.

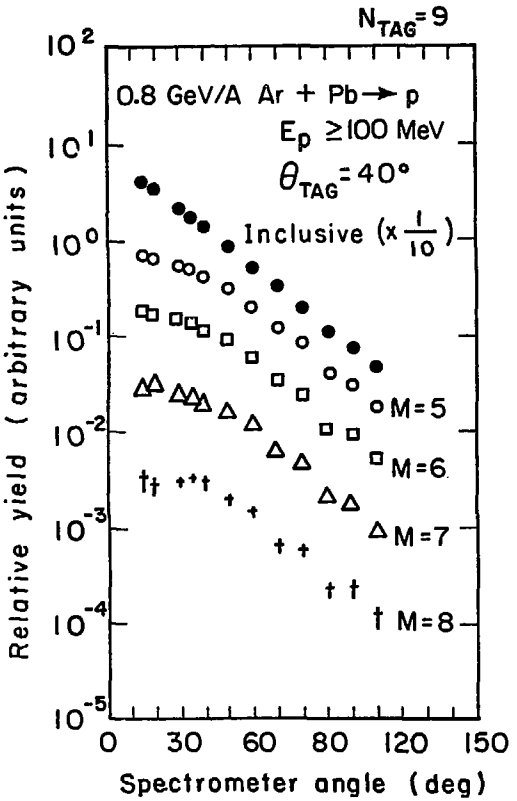

XBL788-1586

Fig.17 Proton angular distributions as a function of the tag-counter multiplicity(M).

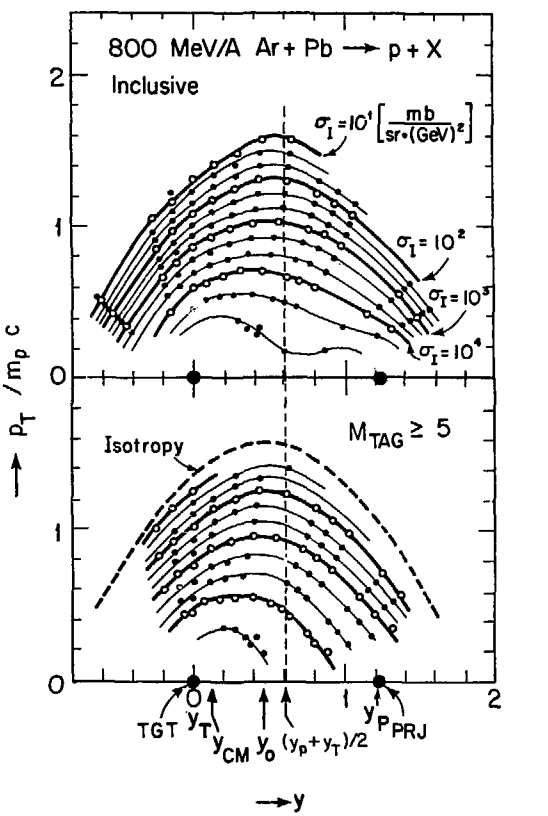

XBL797-2126

Fig.18 Proton spectra in 800-MeV/nucleon Ar + Pb for inclusive(above) and high-multiplicity (below) evens, in the plane of rapidity y and transverse momentum (P_T/m_pC).

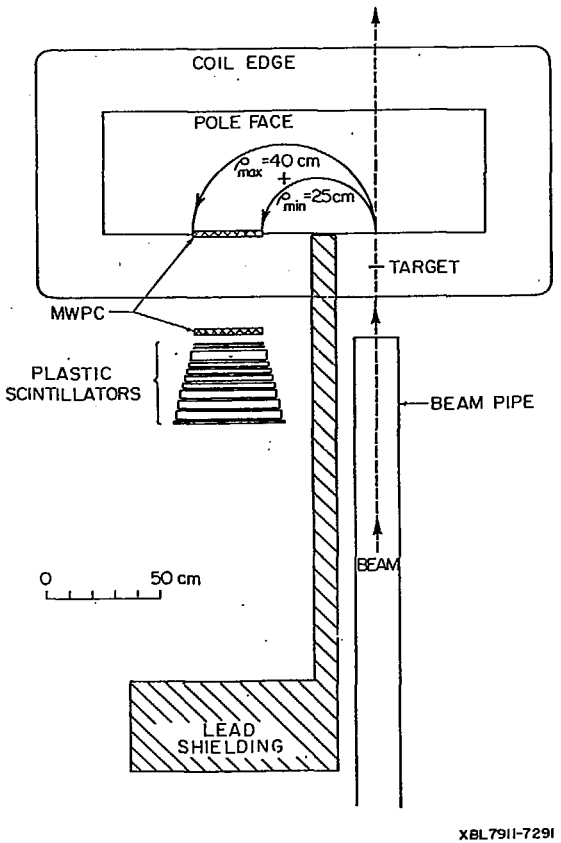

Fig.19 Experimental setup for pion production at 0° in nuclear collisions.

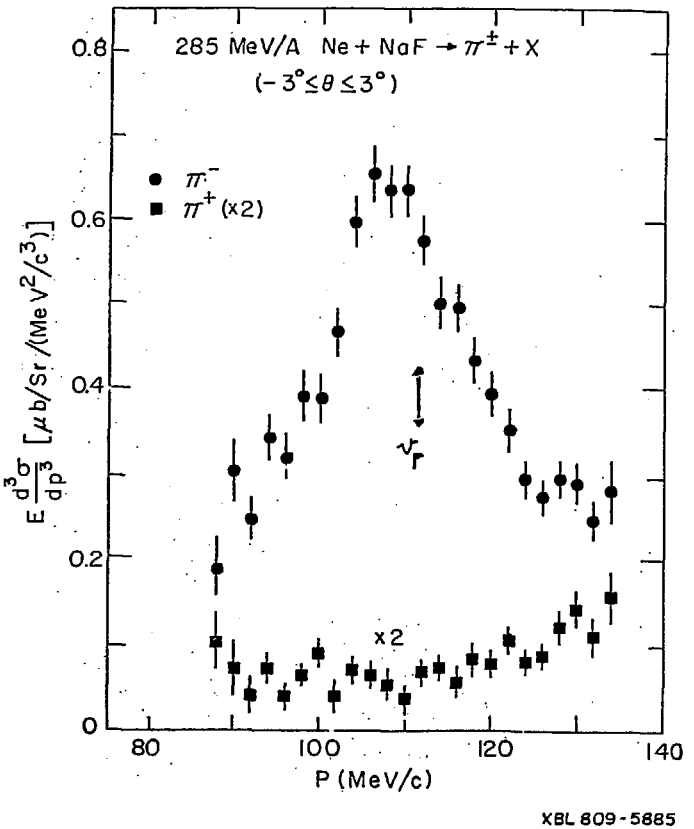

Fig.20 Pion-momentum spectra at 0° in 285-MeV/nuclion Ne + NaF collisions.

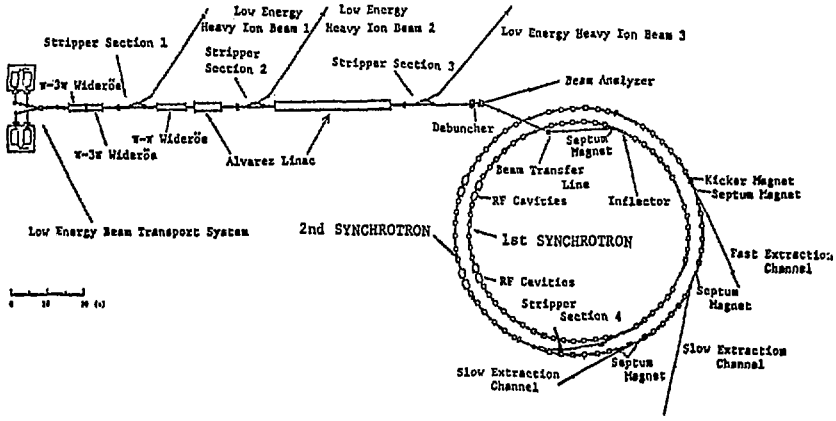

Layout of NUMATRON

Fig.21 Plan view of the Numatron, the proposed high-energy heavy-ion accelerator.

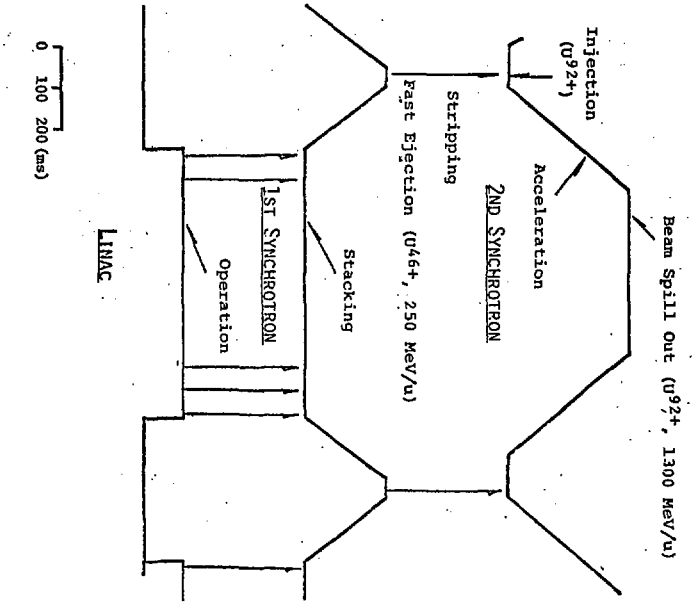

Fig.22 Operation scheme of the Numatron.

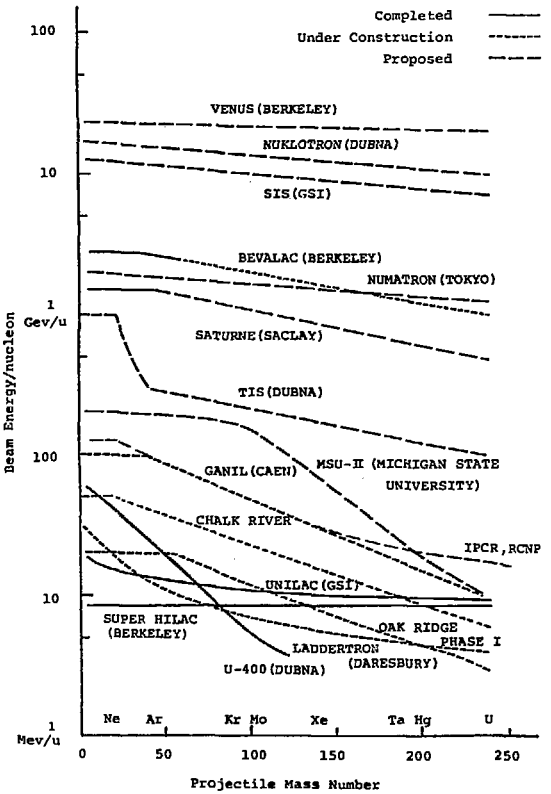

Fig.23 Ion-mass vs. energy capability of the Numatron, together with that of the other existing or proposed projects.

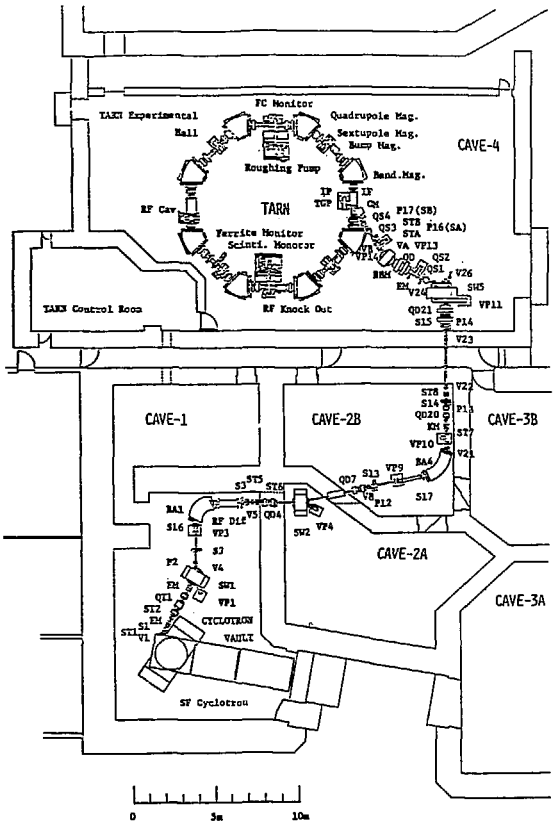

Fig.24 Layout of the test accumulation ring, Tarn, and the beam transport system from the SF cyclotron.

Fig.25 Numatron miniature